Issues in the Dynamics and Control of Flexible Robot Manipulators

H. Baruh* and S. S. K. Tadikonda†
Rutgers University, New Brunswick, New Jersey

Issues associated with modeling and control of robots with elastic arms are considered. An approach similar to substructure synthesis is used to model the system, where each link is first modeled independently of the others. The joint displacements are then used as constraints to synthesize the equations of motion. It is shown that the centrifugal stiffening effect is the dominating factor for the overall system behavior. Different approaches are discussed for the control design. The effects of flexibility on the response and on the closed-loop control are examined within the context of an example.

I. Introduction

An important issue of concern in the control of robots is the difference between the total mass of the manipulator and the mass of the payload. If a robot is compared with the human body, it is easily concluded that the manipulator is very inefficient. An inefficient robot implies low productivity and higher costs. A robot can be made more efficient by reducing the thickness of its arms. The resulting increased flexibility, unless considered properly, reduces pointing accuracies and affects the stability of the payload. Another source of inaccuracy is flexibility of the joints. There is considerable debate in the literature as to which source causes more inaccuracies.

This paper is concerned with the modeling and control of manipulators with substantial flexibility in the arms. An approach similar to substructure synthesis is used to model the manipulator, and different control strategies are discussed. The mathematical formulation is applicable to robots with revolute or spherical joints.

Several methods of modeling manipulators with elastic joints or with flexible arms exist in the literature.[1-11] Each of the approaches uses a variety of assumptions. For example, Refs. 1-4 consider only the static deflections of the links; Ref. 1 treats the connecting links as massless, and Ref. 4 considers only one flexible bending mode for each link. Reference 7 describes an equivalent rigid-link system. Passive damping is introduced to elastic members in Ref. 8, in the form of a layer of viscoelastic material. Active control of the combined rigid-elastic system is considered in Refs. 8 and 9, where Ref. 8 also reports experimental results. Reference 10 introduces a recursive analysis to formulate the equations of motion. A method for modeling joint elasticity is outlined in Ref. 12.

Another issue of concern in modeling a flexible manipulator, which has not been analyzed in detail, is the real-time applicability of the control action. The mathematical model should lend itself to efficient on-line computations when implementing the control action.

In this paper, the nonlinear equations of motion are derived using an approach similar to that in Refs. 13 and 14, and a small motions assumption is employed to describe the elastic behavior. Each link is modeled independently by means of a body-fixed frame that indicates the location of the link in the absence of elastic motion. The joint displacements are then used as constraints to derive the combined equations of motion in a manner similar to the component mode and substructure synthesis methods.[15] The relative effects of centrifugal stiffening, softening, and Coriolis effects are discussed.

After the equations of motion are derived, the control action is considered. When designing a control law to maneuver the robot, one can treat the flexibility of the robot arms in the following ways: 1) ignore it completely, 2) treat the elastic effects as a known disturbance and compensate for it, and 3) actively control the flexible motion.

Ignoring the elastic motion leads to deterioration in tracking accuracy, especially as the flexibility increases. An effective active control of the elastic motion requires a large number of actuation mechanisms that have to be placed on the robot arms.[16] This is difficult to implement, considering the weight of the actuation mechanisms and speed of the manipulator arms. However, local control of the elastic motion has been considered for industrial applications.

The approach used in this paper is to treat the flexibility as a deterministic disturbance on the rigid-body motion. It is shown that ignoring the arm elasticity in the control law leads to gross inaccuracies in the response. The flexible motion is treated similar to the way the gravitational, Coriolis, and centrifugal effects are treated in the computed torque method,[17] pointwise-optimal control of rigid manipulators,[18] or in the nonlinear inversion algorithm of Ref. 19. The feedback control law used in the paper is based on the approach of Ref. 18, and it is implemented by spatially distributed sensors that measure the elastic motion.

II. Equations of Motion

Consider a chain of l elastic bodies linked to each other. One end of the chain is pinned to a rigid support, and the other end is free. To derive the equations of motion, we will use a Lagrangian approach and consider each link independently. After writing the kinetic and potential energies and the virtual work associated with each body, the joint displacements will be treated as constraints.

The displacement of each elastic body is described with respect to a coordinate frame that is located at the center of mass of the undeformed link. Note that for a free-free structure, the elastic motion does not effect the location of the center of mass.[13] This coordinate frame is referred to as the "shadow frame" in Ref. 20, and it denotes the location of the body if there was no flexible motion.[13,14] Moreover, it is assumed that the body axes are aligned with the principal axes of the undeformed link. The link configuration is shown in Fig. 1.

Presented at the VPI&SU/AIAA Symposium on Dynamics and Control of Large Structures, Blacksburg, VA, June 29-July 1, 1987; received Sept. 21, 1987; revision received June 14, 1988.

*Assistant Professor, Department of Mechanical and Aerospace Engineering. Member AIAA.

†Graduate Assistant, Department of Mechanical and Aerospace Engineering. Student Member AIAA.

The displacement of a point P_j on the jth link can be expressed as

$$r_j(P_j,t) = R_j(t) + r_{jB}(P_j) + u_j(P_j,t), \qquad j = 2,3,\ldots,l \quad (1)$$

where $R_j(t)$ is the vector from an inertial frame to the origin of the body-fixed frame, $r_{jB}(P_j)$ denotes the configuration of point P_j (in the undeformed position), and $u(P_j,t)$ is the elastic deformation at P_j. For the first link, $j = 1$, which is pinned to a support, one can select a coordinate frame whose origin is at the support, such that the displacement $r_1(P_1,t)$ is described as

$$r_1(P_1,t) = r_{1B}(P_1) + u_1(P_1,t) \quad (2)$$

It follows that in this case one does not deal with the center of mass of the first link. If the support moves, such as the robot arm in the Space Shuttle, an additional term is added to the right side of Eq. (2) describing this motion.

Details about the motivation to express the displacements in this form are described in Ref. 14. The most important reason is based on the assumption that the elastic motion is small, and that $u_j(P_j,t)$ can be expressed as

$$u_j(P_j,t) = \sum_{r=1}^{\infty} \phi_{jr}(P_j)u_{jr}(t), \qquad j = 1,2,\ldots,l \quad (3)$$

where $\phi_{jr}(P_j)$ $(r = 1,2,\ldots)$ are admissible functions describing the flexible behavior of the jth body. Note that as a result of expressing the total motion in terms of R_j and $r_{jB}(P_j)$, we have introduced six additional coordinates to the system description, which creates a redundancy. One way of dealing with this redundancy is to introduce constraints on the location and orientation of the body frame. To this end, a number of choices are available, such as the principal axes, Tisserand, or rigid-body constraints.[21,22] In this paper we will use the latter constraints, which state that the body frame must have its origin at the center of mass of the deformed structure, and it must be aligned such that the rigid-body modes in Eq. (3) are all zero. This eliminates the six coordinates belonging to the rigid-body modes, $u_{jr}(t) = 0$ $(r = 1,2,\ldots,6)$, so that there no longer is a redundancy in the expression of $r_j(P_j,t)$.

The preceding model for the elastic motion is only accurate when the links (and, hence, the body-fixed frames) move relatively slowly. For fast motions of the links, the centrifugal stiffening effect has to be considered as well, where Eq. (3) changes form. This effect will be described in more detail later within the context of an example.

Differentiation of Eqs. (1) and (2) with respect to time yields the absolute velocities

$$\dot{r}_j(P_j,t) = \dot{R}_j(t) + \mathrm{d}u_j(P_j,t)/\mathrm{d}t + \Omega_j(t) \times [r_{jB}(P_j) + u_j(P_j,t)], \qquad j = 1,2,\ldots,l \quad (4)$$

where Ω_j denotes the absolute angular velocity of the jth coordinate frame. The kinetic energy of the entire system can be expressed as

$$K(t) = \sum_{j=1}^{l} K_j(t) \quad (5)$$

where

$$K_j(t) = \tfrac{1}{2}\int \dot{r}_j(P_j,t) \cdot \dot{r}_j(P_j,t)\, \mathrm{d}m_j, \qquad j = 1,2,\ldots,l \quad (6)$$

denotes the kinetic energy of the jth link, and where $\mathrm{d}m_j$ is the differential mass at P_j. The potential energy can be expressed as

$$V(t) = \sum_{j=1}^{l} [V_{je}(t) + V_{jg}(t)] \quad (7)$$

where

$$V_{je}(t) = \tfrac{1}{2}\int u(P_j,t) \cdot L_j[u(P_j,t)]\, \mathrm{d}m_j, \qquad j = 1,2,\ldots,l \quad (8)$$

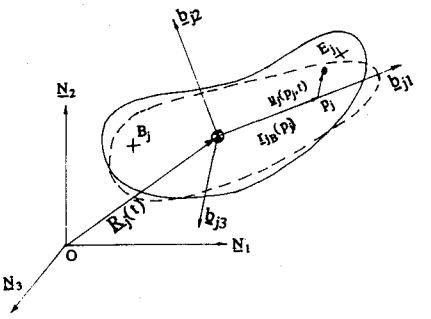

Fig. 1 Configuration of a flexible link.

is the elastic potential energy of the jth link in which L_j denotes the vector stiffness operator associated with the jth link. Because of the small elastic motions assumptions, $L_j(j = 1,2,\ldots,l)$ are linear. The gravitational potential energy has the form

$$V_{jg}(t) = -\int r_j(P_j,t) \cdot g\, \mathrm{d}m_j, \qquad j = 1,2,\ldots,l \quad (9)$$

where g is the gravity vector.

For the general formulation, consider spatially continuously distributed controllers on each link in the form of distributed forces $f_j(P_j,t)$, $(j = 1,2,\ldots,l)$, and distributed moments $M_j(P_j,t)$, $(j = 1,2,\ldots,l)$. The virtual work expression becomes

$$\delta W = \sum_{j=1}^{l} \delta W_j \quad (10)$$

where[14]

$$\delta W_j = \int f_j(P_j,t) \cdot \delta r_j(P_j,t)\, \mathrm{d}m_j + \int M_j(P_j,t) \cdot [\nabla \times \delta r_j(P_j,t)]\, \mathrm{d}m_j \quad (11)$$

Next, we consider the constraints. Assuming that all the joints are revolute, the displacement constraints can be expressed as

$$c_j(t) = r_j(E_j,t) - r_{j+1}(B_{j+1},t) = 0, \qquad j = 1,2,\ldots,l-1 \quad (12)$$

where $c_j(t)$ is the constraint relation, and E_j and B_j denote the locations of the joints on the jth link (see Fig. 1). If a certain joint is further constrained, such as permitting rotation about a single axis only, Eq. (12) can be augmented with additional relations, or $r_j(P_j,t)$ can be expressed in a way to reflect this constraint. For example, for the $j + 1$th link denoting the orientation of the body-fixed frame by the unit vectors b_1, b_2, and b_3, if the jth joint is free to rotate about the b_1 axis only, we need the additional constraints

$$[\nabla \times r_j(P_j,t)|_{P_j = E_j} - \nabla \times r_{j+1}(P_{j+1},t)|_{P_{j+1} = B_{j+1}}] \cdot b_i = 0, \qquad i = 2,3 \quad (13)$$

which indicate that there is no rotation at the jth joint about the b_2 and b_3 directions. Note that, as in Eq. (11), the Del operator is defined in terms of the body-fixed coordinates. Introducing the augmented Lagrangian L'

$$L' = K - V + \sum_{j=1}^{l-1} \lambda_j \cdot c_j \quad (14)$$

where λ_j are Lagrange multiplier vectors and, invoking the extended Hamilton's principle,[23] we obtain a set of redundant equations. To synthesize the equations of motion, we need to select a set of generalized coordinates. Here, two issues emerge. The first is associated with the description of the elastic motion of each link. The second issue is associated with eliminating some of the coordinates from the equations ob-

tained using Eq. (14) and with satisfying the constraint relations. We address each issue in sequence.

The elastic motion $u_j(P_j,t)$ of each link is approximated as a finite sum of admissible functions $\phi_{jr}(P_j)$ multiplied by the amplitudes $u_{jr}(t)$

$$u_j(P_j,t) = \sum_{r=1}^{N_j} \phi_{jr}(P_j)u_{jr}(t), \qquad j = 1,2,...,l \tag{15}$$

where N_j is the number of terms in the expansion of $u_j(P_j,t)$. Note that the trial functions ϕ_{jr} now only describe the elastic motion because the rigid-body modes are eliminated from the equations of motion by a judicious choice of the body-fixed frame. It follows that the elastic potential energy can be expressed as

$$V_{je}(t) = \frac{1}{2}\sum_{r=1}^{N_j}\sum_{s=1}^{N_j}[\phi_{jr},\phi_{js}]\, u_{jr}(t)u_{js}(t), \qquad j = 1,2,...,l \tag{16}$$

where $[\phi_{jr},\phi_{js}]$ is an energy inner product.[15] Equations (15) and (16) have a different form when the effects of centrifugal stiffening are included, as will be shown later.

Regarding the nature of the admissible functions, we note that it is simpler not to search for a set of eigenfunctions for each link.[15] Also, for convergence purposes, it is more desirable to use admissible functions that are compatible with the system force balance. Consider the boundaries of each link. The boundary conditions at a free end are natural boundary conditions where the bending moment and internal force are zero. Imposition of a constraint of the form in expression (12) changes the boundary conditions. The internal force is no longer zero at that point. Use of trial functions such as the original eigenfunctions of the individual links, which yield zero shear at a pin joint, prohibits convergence to the exact eigensolution. This, of course, is the very reason why constraint or attachment modes are introduced to the system description in the component mode synthesis method.[24] The preceding formulation is more similar to the substructure synthesis method.[25]

The coordinates used in Eq. (14) are the components of $\boldsymbol{R}_j(t)$ $(j = 1,2,...,l)$, the three (or fewer, depending on the joint constraints) angles ϕ_j, θ_j, ψ_j for each coordinate frame that describe the orientation of each link, and the modal coordinates $u_{jr}(t)$ $(j = 1,2,...,l;\ r = 1,2,...,N_j)$. The angles ϕ_j, θ_j, ψ_j can be any sequence from an Euler angle set, and the vectors $\boldsymbol{\Omega}_j(t)$ are obtained by their differentiation. If desired, Euler parameters can be substituted instead of the coordinate frame angles to minimize problems associated with numerical integration.

We need to eliminate some of these coordinates so that the constraint relations are satisfied and the remaining variables can qualify as a set of generalized coordinates. We propose first to eliminate $\boldsymbol{R}_j(t)$ $(j = 1,2,...,l)$. This is a logical choice because we are not interested in the location of the center of mass of each link for modeling purposes. Also, the number of constraint relations in Eq. (12) is equal to the total sum of the components of $\boldsymbol{R}_j(t)$ $(j = 1,2,...,l)$.

If constraints of the form in expression (13) are present at the jth joint, then the coordinates to be eliminated should be the corresponding rotation angles of the $j+1$th body frame. Note that the angles on which the control action will be based are not joint displacements, but the angles that describe the orientations of the coordinate frames in the absence of gravity and static deformation. Any angle between two links measured at the joints contains flexibility effects, and these effects need to be filtered out before the control law can be applied.

Introducing the m-dimentional vector $\theta(t)$, which contains all of the coordinate frame angles that are not redundant, and the k-dimensional vector $v(t)$ $(k = N_1 + N_2 ... + N_l)$ containing all of the elastic modes of the individual links

$$v(t) = [u_{11}u_{12}...u_{1,N_1}u_{21}u_{22}...u_{l,N_l}]^T \tag{17}$$

and the n-dimensional vector $y(t) = [\theta^T(t)\,|\,v^T(t)]^T$, which contains the generalized coordinates where $n = m + k$, and eliminating the redundant terms $\boldsymbol{R}_j(t)$, the equations of motion can be expressed as

$$M[y(t)]\ddot{y}(t) + G[\dot{y}(t),y(t)] = F(t) \tag{18}$$

where M is the inertia matrix, $G = [G_1G_2...G_n]^T$, where G_i contain the Coriolis, centrifugal, graviational, elastic, and centrifugal stiffening effects. $F(t) = [F_1(t)F_2(t)...F_n(t)]^T$ denote the generalized forces. The virtual work can be expressed in terms of the generalized forces as

$$\delta W = F^T\delta y \tag{19}$$

It is more convenient for simulation and control purposes to partition Eq. (18) into the body frame angle dependent and elastic terms as

$$\begin{bmatrix} M_{\theta\theta} & M_{\theta v} \\ M_{v\theta} & M_{vv} \end{bmatrix}\begin{bmatrix} \ddot{\theta}(t) \\ \ddot{v}(t) \end{bmatrix} + \begin{bmatrix} G_\theta(t) \\ G_v(t) \end{bmatrix} = \begin{bmatrix} F_\theta(t) \\ F_v(t) \end{bmatrix} \tag{20}$$

where the notation is obvious. For discrete torquers at the ends B_j of each link $(j = 1,2,...,l)$, the external excitation can be expressed as

$$M_j(P_j,t) = \Sigma T_{ji}(t)\boldsymbol{b}_{ji}\delta(P_j - B_j), \qquad j = 1,2,...,l, \quad i = 1,2,3 \tag{21}$$

where $T_{ji}(t)$ $(j = 1,2,...,l;\ i = 1,2,3)$ are the torque amplitudes in the jth link and in the $\boldsymbol{b}_{ji}$ direction, and $\boldsymbol{b}_{ji}$ denotes the body axes about which motion is permitted at the jth joint. Substitution of Eq. (21) into Eqs. (10) and (19) yields

$$F(t) = BT(t) \tag{22}$$

where B is the control influence matrix of order $n \times p$, and $T(t)$ is the external excitation vector in the form $T(t) = [T_1(t)T_2(t)...T_p(t)]^T$ in which p is the number of rigid-body degrees of freedom. Note that in robots with rigid arms there is generally one actuator per degree of freedom. The matrix B can be partitioned into $B = [B_\theta^T\,|\,B_v^T]^T$, corresponding to the rigid-body and elastic motion, respectively. When $p = m$, B_θ becomes an identity matrix.

As can be noted, the preceding derivation is very general, and it does not give details about the type of coordinate frame angles used. The complexity of the geometry and the vast variety of existing robots prevents us from making the derivation more specific. Also, if desired, the gravitational and elastic terms can be collected in a stiffness matrix. We did not follow this approach. In general, for rigid robots, the control strategy treats the centrifugal, Coriolis, and gravitational terms as a deterministic disturbance (even when the magnitudes of these terms are large), which has come to be known as "feedforward control." In this paper, we include the elastic terms into this category of deterministic disturbances.

III. Control Design and Implementation

The objective in manipulator control is to move the end effector from a certain point to a desired one with a specified speed and in a specified amount of time (e.g., Refs. 17, 18, and 26). This can be achieved in a number of ways. In this paper, we will consider trajectory-following.

In manipulators with rigid arms, the joint angles (and angular velocities and angular accelerations) are measured by colocated sensors at the joints and sometimes also by sensors located at the end effector. The actuators, which generally are torquers, are also located at the joints. The tracked coordinates are the joint displacements and velocities, so that the control inputs are designed to realize the desired link con-

figurations.[18] We will refer to two approaches in trajectory-following for rigid robots, whose equation of motion can be expressed as

$$M'(q)\ddot{q}(t) + G'(q,\dot{q}) = T(t) \tag{23}$$

where $q(t)$ denotes the vector of joint angles, M' is the inertia matrix, and G' includes all Coriolis, centrifugal, and gravitational terms. In the absence of any elastic motion, $q(t) = \theta(t)$, $M' = M_{\theta\theta}$, $G' = G$, and $T(t) = F(t)$.

The first control method to be considered is the computed torque method,[17,26] where the control action can be described as

$$T(t) = M'\{\ddot{q}_a(t) + C_1[\dot{q}_a(t) - \dot{q}(t)] + C_2[q_a(t) - q(t)]\} + G'(t) \tag{24}$$

where C_1 and C_2 are diagonal control gain matrices, and the subscript a denotes desired coordinates. Note that displacements, velocities, and accelerations are all tracked. In the computed torque method, the equations of motion are first linearized via feedback [$\ddot{q}_a(t)$ and $G'(t)$ in Eq. (24)]. Then, a servomechanism is added to the feedback-linearized equations.[26]

In the second approach considered here, the control law may or may not include acceleration tracking, the discrete (in time) nature of the control implementation is considered, and the control gains are derived from a pointwise-optimal control law.[18] The inertia matrix and Coriolis, gravitational, and centrifugal terms are approximated by a constant during each sampling period, which permits consideration of the equations of motion as linear during each sampling period. It follows that in each sampling period an approximate closed-form expression can be derived for the response as

$$q(kT + T) = q(kT) + \dot{q}(kT)^*T + 0.5F'(kT)^*T^2,$$
$$\dot{q}(kT + T) = \dot{q}(kT) + F'(kT)^*T, \qquad k = 0,1,2... \tag{25}$$

where T is the sampling period, and $F'(kT) = M^{-1}(kT)T(kT) + d'(kT)$, where $d'(kT)$ is an approximation to the Coriolis, centrifugal, and graviational terms. Substitution of this approximate form of the response into a quadratic performance index that minimizes the tracking error leads to a control law in the form[18]

$$T(kT) = M'(kT)\{C_1[\dot{q}_a(kT + T) - \dot{q}(kT)] + C_2[q_a(kT + T) - q(kT)] + C_3\dot{q}(kT) + C_4d'(kT)\}, \qquad k = 0,1,2,... \tag{26}$$

in which C_1, C_2, C_3, and C_4 are control gain matrices derived from a performance functional.[18]

The two control methods perform comparably, but the control described by Eq. (26) is more robust in the presence of parameter uncertainties and it can be formulated to take into consideration the delay in the control application by estimating the system state one time step ahead.[18] Note that the effects of a one (or more) time step delay in the control application are very critical for robot motion control.[18]

For flexible manipulators, the trajectory-following problem becomes one of specifying not the desired link configurations, but one of specifying the desired orientations of the body-fixed coordinate frames. Also, measurement of the angle between two links at a joint represents the sum of the angle between the two coordinate frames and the slopes of the elastic deformations at the joints in the form

$$q(t) = \theta(t) + \nabla \times u_B(t) - \nabla \times u_E(t) \tag{27}$$

where $u_B(t) = [u_1^T(B_1,t)u_2^T(B_2,t)...u_l^T(B_l,t)]^T$ and $u_E(t) = [0^T u_1^T(E_1,t)...u_{l-1}^T(E_{l-1},t)]^T$ contain the elastic amplitudes at the beginning and end of each link, respectively. The process of extracting the reference frame angles from the measured angles between two elastic links will be discussed later.

We can identify three approaches for trajectory-following in elastic manipulators:

1) Elastic effects are ignored. Here, it is assumed that the equation of motion is Eq. (23). Not only is the mathematical model incorrect in this case, but the control inputs are calculated using the angles between the links given by Eq. (27) instead of the coordinate frame angles. Trajectory-following control laws such as computed torque or pointwise-optimal control are generally very sensitive to inaccuracies in the measurements of the joint angles, so that ignoring the elastic behavior of the links may result in gross inaccuracies.

2) The elastic effects are included in the mathematical model to a certain extent, and their amplitudes are measured or extracted from the sensors' measurements, but the elastic motion is not explicitly controlled. In this case the effects of the elastic deformation are treated as known disturbances. Here, a variety of approaches can be considered depending on how much one wishes to consider the contribution of the elastic motion. For example, one approach is as follows: Assuming that the manipulator is operated in a gravity-free environment, so that the static deformation is zero, Eq. (20) can be rearranged as

$$(M_{\theta\theta} - M_{\theta v}M_{vv}^{-1}M_{v\theta})\ddot{\theta}(t) + (G_\theta - M_{\theta v}M_{vv}^{-1}G_v) = F_\theta(t) - M_{\theta v}M_{vv}^{-1}F_v(t) \tag{28}$$

The control vector in Eq. (28) is of the same order as the rigid-body degrees of freedom. Consequently, control strategies based on computed torque [Eq. (24)] or pointwise-optimal [Eq. (26)] control can be adopted. The first term in Eq. (28) is seen as the inertia matrix, the second term as the deterministic disturbance consisting of the Coriolis, centrifugal, and elastic effects, while the term on the right side of Eq. (28) is considered the input.

Another approximation is based on considering only the top row of Eq. (20) and treating $M_{\theta v}v(t)$ as a deterministic disturbance, resulting in

$$M_{\theta\theta}\ddot{\theta}(t) + [G_\theta + M_{\theta v}\ddot{v}(t)] = F_\theta(t) \tag{29}$$

and to use a control design similar to computed torque or pointwise-optimal control. Not using the bottom row of Eq. (20) is equivalent to assuming that the excitation caused by the rigid-body motion on the elastic motion is negligible.

Yet another approach is to use the equations of motion for the equivalent rigid robot, [Eq. (23)] as the model and, when designing the control law, to use as coordinates not the measured angles but the body frame angles calculated by Eq. (27). This approach minimizes the number of on-line computations required to determine the control input.

The feedback control approaches considered in the illustrative examples are based on the aforementioned cases. Note that other approximations that take the elastic effects into consideration also can be developed.

3) The elastic motion is suppressed simultaneously with the trajectory-following. Here, as mentioned earlier, one can expand the elastic and gravitational effects in a stiffness matrix or keep the formulation in Eq. (20). Expansion of the gravity and elastic effects in a stiffness matrix necessitates solution of an eigenvalue problem at each time step of the control, which creates additional computational burdens.

One way of suppressing the elastic motion is to attempt a control law similar to Eqs. (24) or (26). However, to apply either of these methods, the number of control inputs has to be equal to the number of controllers, which necessitates placement of n-k additional actuators along the robot. Con-

sidering the current state of the art, it seems unfeasible to achieve this, even though in some industrial applications a small number of energy-absorbing actuators have been placed on the manipulator arms.

If the total number of actuators is increased to n and a control law similar to Eq. (26) is used, the control input becomes

$$T(kT) = B^{-1}(kT)M(kT)\{C_1[\dot{y}_a(kT+T) - \dot{y}(kT)] + C_2[y_a(kT+T) - y(kT)] + C_3\dot{y}(kT) + C_4 d'(kT)\}, \qquad k = 0,1,2,\ldots \tag{30}$$

where we note that $d'(kT)$ is now of order n, and that the actuation mechanisms need to be placed such that B is nonsingular. Implementation of the control requires synthesis of the torque amplitudes, which presents two problems. The first deals with extraction of the coordinate frame angles, and the second with obtaining elastic mode amplitudes from the system measurements. Note that even though the elastic motion is not controlled, it is treated as a disturbance in Eqs. (28) and (29), so that its amplitude needs to be known.

Another important issue associated with real-time implementation is the huge number of required computations. Calculation of the dynamics of rigid robots does not pose a severe burden anymore,[26] but the number of calculations involved in elastic robots is much larger. To tackle this problem one may make use of parallel computing techniques. Also, not suppressing the elastic motion actively reduces the number of on-line computations.

IV. Illustrative Examples

As an illustration, we derive here the equations of motion for a two-link manipulator, shown in Fig. 2. The manipulator has three kinematic degrees of freedom: one each at the revolute joints, and a base rotation. Each link is modeled as a uniform slender bar of length L_j and mass m_j ($j = 1,2$). The joints are assumed to be rigid and frictionless.

N_i ($i = 1,2,3$) are a set of inertial axes, and they also represent unit vectors along those axes. The body-fixed axes b_{ji} ($i = 1,2,3$) in the jth link are located such that b_{j1} points along the link length, and b_{j3} is parallel to the joint axis at B_j of the "shadow" beam; u_{jx}, u_{jy}, and u_{jz}, are the components of u_j along b_{j1}, b_{j2}, and b_{j3}, respectively, where x is the local spatial variable. The origin of the body-fixed axes is placed at the revolute joint connecting it to the base for the first link and is located at the mass center for the second link.

The displacement at a point P on the first link can be expressed as

$$r_1(P,t) = [x + u_{1x}(x,t)]b_{11} + u_{1y}(x,t)]b_{12} + u_{1z}(x,t)\ ]b_{13} \tag{31}$$

The absolute velocity is

$$\dot{r}_1(P,t) = \frac{du_{1x}}{dt}b_{11} + \frac{du_{1y}}{dt}b_{12} + \frac{du_{1z}}{dt}b_{13} + (\dot{\theta}_1 + \dot{\psi}) \times r_1(P,t) \tag{32}$$

where $\dot{\theta}_1 = \dot{\theta}_1 b_{13}$ and $\dot{\psi} = \dot{\psi}N_2$.

The term u_{1x} contains contributions from both the axial vibration of the link and centrifugal stiffening. To analyze this effect, consider an element of length ds whose undeformed length is dx as shown in Fig. 3[27]:

$$d\xi = \left[1 - \left(\frac{\partial u_{1y}}{\partial x}\right)^2 - \left(\frac{\partial u_{1z}}{\partial x}\right)^2\right]^{1/2} ds \tag{33}$$

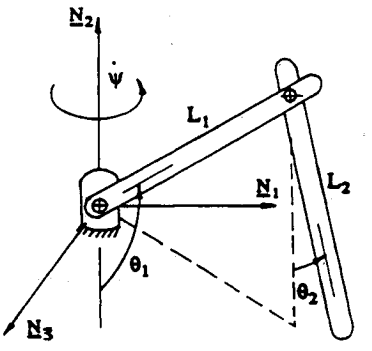

Fig. 2 Three-degree-of-freedom manipulator.

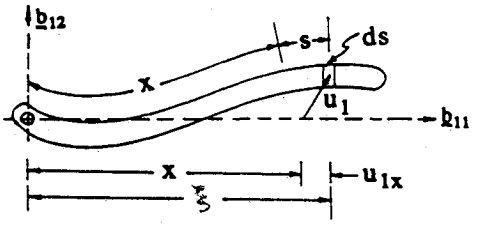

Fig. 3 Pinned-free link.

Integrating and making use of the property that u_{1y} and u_{1z} are small,

$$\xi = x + s(x,t) - \frac{1}{2}\int_0^{x+s(x,t)} \left[\left(\frac{\partial u_{1y}}{\partial \sigma}\right)^2 + \left(\frac{\partial u_{1z}}{\partial \sigma}\right)^2\right] d\sigma \tag{34}$$

Since $\xi = x + u_{1x}$ from Fig. 3,

$$u_{1x}(x,t) \approx s(x,t) - \frac{1}{2}\int_0^{x+s(x,t)} \left[\left(\frac{\partial u_{1y}}{\partial \sigma}\right)^2 + \left(\frac{\partial u_{1z}}{\partial \sigma}\right)^2\right] d\sigma \tag{35}$$

where $s(x,t)$ denotes the "stretch" along the deformed beam due to axial vibration. The reason for expressing $u_{1x}(x,t)$ as a sum of two components is to compare the contributions of longitudinal vibration and centrifugal stiffening to elastic deformation in the axial direction. The integral in Eq. (35), when substituted into Eq. (5), gives rise to the centrifugal stiffening term. Its magnitude may be comparatively large and, since modal expansion is valid only for small displacements, of the two terms in Eq. (35) only $s(x,t)$ can be represented by a modal expansion.[20] We assume that the manipulator links are much more rigid in the longitudinal direction than in the transverse direction, and drop $s(x,t)$ in further development.

Equation (3) now has the form

$$u_1(x,t) = u_{1x}b_{11} + \sum_{i=1}^{N_1} \phi_{1i}u_{1i} \tag{36}$$

where

$$\phi_{1i} = \phi_{1i}b_{12}, \qquad i \le N_{11}$$
$$= \phi_{1i}b_{13}, \qquad N_{11} < i \le N_1 \tag{37}$$

N_{11} and $N_{12} = N_1 - N_{11}$ are the number of terms in the expansion in the y and z directions, respectively.

Substituting $\dot{r}_1$ from Eq. (32) and the modal expansion of Eq. (36) into Eq. (5), and retaining terms only up to quadratic

in modal coordinates, the kinetic energy of the first link is obtained as

$$
\begin{aligned}
2K_1 &= m_{ij}^{(1)}\dot{u}_{1i}\dot{u}_{1j} + m_{kl}^{(1)}\dot{u}_{1k}\dot{u}_{1l} + I_1(\dot{\theta}_1^2 + \dot{\psi}^2\sin^2\theta_1) \\
&+ [(m_{ij}^{(1)} - h_{ij}^{(1)})\dot{\theta}_1^2 + (m_{ij}^{(1)}\cos^2\theta_1 - h_{ij}^{(1)}\sin^2\theta_1)\dot{\psi}^2]u_{1i}u_{1j} \\
&+ [m_{kl}^{(1)}\dot{\psi}^2 - h_{kl}^{(1)}(\dot{\theta}_1^2 + \dot{\psi}^2\sin^2\theta_1)]u_{1k}u_{1l} \\
&+ 2\dot{\psi}\dot{\theta}_1(f_{1k}u_{1k}\cos\theta_1 - m_{ik}^{(1)}u_{1i}u_{1k}\sin\theta_1) \\
&+ 2\dot{\psi}[\cos\theta_1 m_{ij}^{(1)}(\dot{u}_{1i}u_{1k} - u_{1i}\dot{u}_{1k}) - \sin\theta_1 f_{1k}\dot{u}_{1k}] \\
&+ 2f_{1i}\dot{u}_{1i}\dot{\theta}_1 + f_{1i}u_{1i}\dot{\psi}^2\sin 2\theta_1
\end{aligned} \tag{38}
$$

where I is the moment of inertia about the pin joint,

$$
m_{ab}^{(1)} = \int \phi_{1a}\phi_{1b}\,\mathrm{d}m
$$

$$
h_{ab}^{(1)} = \int x\int_0^x \phi_{1a}'\cdot\phi_{1b}'\,\mathrm{d}\sigma\,\mathrm{d}m, \qquad f_{1a} = \int x\phi_{1a}\,\mathrm{d}m \tag{39}
$$

and Einstein's summation convention has been employed for conciseness. The range of indices is $1 \le i,j \le N_{11}$, $(N_{11}+1) \le k,l \le N_1$, and $1 \le a,b \le N_1$.

The potential energy of the first link is

$$
\begin{aligned}
V_1 &= \tfrac{1}{2}\,k_{ab}^{(1)}u_{1a}u_{1b} - m_1 g\,(L_1/2)\cos\theta_1 + g\sin\theta_1 t_{1i}u_{1i} \\
&+ (g/2)\cos\theta_1 e_{ab}^{(1)}u_{1a}u_{1b}
\end{aligned} \tag{40}
$$

where

$$
k_{ab}^{(1)} = \int E_1 I_A(x)\phi_a''\cdot\phi_b''\,\mathrm{d}x, \qquad e_{ab}^{(1)} = \int G_{ab}^{(1)}(x)\,\mathrm{d}m
$$

$$
G_{ab}^{(1)}(x) = \int_0^x \phi_a'\cdot\phi_b'\,\mathrm{d}\sigma, \qquad t_{1i} = \int \phi_{1i}\,\mathrm{d}m \tag{41}
$$

E_1 and I_A are the Young's modulus and area moment of inertia of link 1, respectively. The indicial notation in Eqs. (40) and (41) is the same as that in Eqs. (38) and (39).

Next, we consider the second link. The displacement of a point on the second link can be expressed as (Fig. 4)

$$
\boldsymbol{r}_2(x,t) = \boldsymbol{R}_2 + (x + u_{2x})\boldsymbol{b}_{21} + u_{2y}\boldsymbol{b}_{22} + u_{2z}\boldsymbol{b}_{23} \tag{42}
$$

Differentiating Eq. (42) we obtain

$$
\begin{aligned}
\dot{\boldsymbol{r}}_2(x,t) &= \dot{\boldsymbol{R}}_2 + \dot{\psi}N_2\times\boldsymbol{R}_2 + (\dot{u}_{2x} + \dot{\psi}u_{2z}\sin\theta_2 - \dot{\theta}_2 u_{2y})\boldsymbol{b}_{21} \\
&+ \left[\frac{\mathrm{d}u_{2y}}{\mathrm{d}t} + \dot{\psi}u_{2z}\cos\theta_2 + (x + u_{2x})\dot{\theta}_2\right]\boldsymbol{b}_{22} \\
&+ \left[\frac{\mathrm{d}u_{2z}}{\mathrm{d}t} - \dot{\psi}u_{2y}\cos\theta_2 - (x + u_{2x})\dot{\psi}\sin\theta_2\right]\boldsymbol{b}_{23}
\end{aligned} \tag{43}
$$

To calculate the centrifugal stiffening term $u_{2x}(x,t)$, we use an approach similar to Eqs. (33–35). Because the second link is free at both ends and centrifugal stiffening does not depend on the translational motion, the link can be treated as a structure rotating about its midpoint ($x = 0$), which can be considered as fixed. It follows that the stretch at the midpoint of the beam is zero. Using this result, the centrifugal stiffening term for the second link becomes very similar to the stiffening term for link 1 [Eq. (35)].

Equation (3) is now modified as [setting $s(x,t) = 0$]

$$
u_2(x,t) = u_{2x}\boldsymbol{b}_{21} + \sum_{i=1}^{N_2}\phi_{2i}u_{2i} \tag{44}
$$

where

$$
\begin{aligned}
\phi_{2i} &= \phi_{2i}\boldsymbol{b}_{22}, \qquad i \le N_{21} \\
&= \phi_{2i}\boldsymbol{b}_{23}, \qquad N_{21} < i \le N_2
\end{aligned} \tag{45}
$$

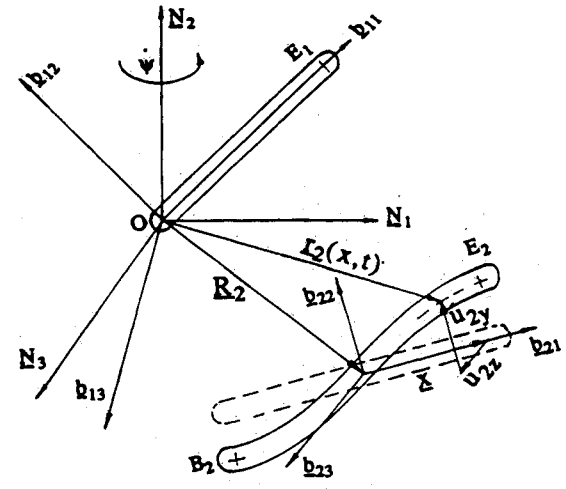

Fig. 4 Configuration of the free-free link.

and N_{21} and $N_{22} = N_2 - N_{21}$ are the number of terms in the expansion of u_{2y} and u_{2z}, respectively.

Substituting Eqs. (44–45) into Eq. (43), we obtain the kinetic energy K_2 of the second link

$$
\begin{aligned}
2K_2 &= m_2[\dot{R}_{21}^2 + \dot{R}_{22}^2 + \dot{R}_{23}^2 + (R_{21}^2 + R_{23}^2)\dot{\psi}^2 \\
&+ 2\dot{\psi}(\dot{R}_{21}R_{23} - R_{21}\dot{R}_{23})] \\
&+ I_2(\dot{\theta}_2^2 + \dot{\psi}^2\sin^2\theta_2) + m_{pq}^{(2)}\dot{u}_{2p}\dot{u}_{2q} + m_{rs}^{(2)}\dot{u}_{2r}\dot{u}_{2s} \\
&+ [m_{pq}^{(2)}(\dot{\theta}_2^2 + \dot{\psi}^2\cos^2\theta_2) - h_{pq}^{(2)}(\dot{\theta}_2^2 + \dot{\psi}^2\sin^2\theta_2)]u_{2p}u_{2q} \\
&+ [m_{rs}^{(2)}\dot{\psi}^2 - h_{rs}^{(2)}(\dot{\theta}_2^2 + \dot{\psi}^2\sin^2\theta_2)]u_{2r}u_{2s} \\
&+ 2\dot{\psi}[\cos\theta_2 m_{pr}^{(2)}(\dot{u}_{2p}u_{2r} - u_{2p}\dot{u}_{2r}) - \sin\theta_2 f_{2p}\dot{u}_{2p}] \\
&+ \dot{\psi}^2\sin 2\theta_2 f_{2p}u_{2p} + 2\dot{\theta}_2 f_{2p}\dot{u}_{2p} \\
&+ 2\dot{\psi}\dot{\theta}_2[\cos\theta_2 f_{2r}u_{2r} - \sin\theta_2 m_{pr}^{(2)}u_{2p}u_{2r}]
\end{aligned} \tag{46}
$$

where I_2 is the moment of inertia about the mass center, and

$$
m_{cd}^{(2)} = \int \phi_{2c}\phi_{2d}\,\mathrm{d}m, \qquad h_{cd}^{(2)} = \int x\int_0^x \phi_{2c}'\cdot\phi_{2d}'\,\mathrm{d}\sigma\,\mathrm{d}m
$$

$$
f_{2p} = \int x\phi_{2p}\,\mathrm{d}m, \qquad R_{2j} = \boldsymbol{R}_2\cdot N_j \qquad (j = 1,2,3) \tag{47}
$$

The range of indices in the Einstein's summation convention employed is $1 \le p,q \le N_{21}$, $(N_{21}+1) \le r,\ s \le N_2$, and $1 \le c,\ d \le N_2$.

The associated potential energy is

$$
\begin{aligned}
V_2 &= \tfrac{1}{2}k_{cd}^{(2)}u_{2c}u_{2d} - \int[\boldsymbol{R}_2 + (x + u_{2x})\boldsymbol{b}_{21} + u_{2y}\boldsymbol{b}_{22} \\
&+ u_{2z}\boldsymbol{b}_{23}]\cdot(-g)N_2\,\mathrm{d}m \\
&= m_2 g R_{22} + \tfrac{1}{2}k_{cd}^{(2)}u_{2c}u_{2d}
\end{aligned} \tag{48}
$$

where

$$
k_{cd}^{(2)} = \int E_2 I_B(x)\phi_{2c}''\cdot\phi_{2d}''\,\mathrm{d}x \tag{49}
$$

and E_2 and I_B are the Young's modulus and area moment of inertia of link 2, respectively. A note about the matrices in Eqs. (38–49) is in order. The mass matrices $m^{(1)}$ and $m^{(2)}$ are fully populated. The rest of the matrices are block diagonal where the blocks represent the vibration in the Y and Z directions, respectively, and the off-diagonal blocks are null matrices.

We next consider the constraints. The two links are connected by a revolute joint. This constraint can be split into displacement and orientation constraints. The latter constraint implies that the plane perpendicular to the joint axis in each link be parallel at the joint connecting them. Here, we assume that the links are already oriented such that Eq. (13) is satisfied ($i = 1,2$), and dispense with the orientation constraints to reduce the amount of algebra involved. This enables one to deal with the body frame angles θ_2 and ψ in a direct fashion.

Because shear and warping are neglected, we need to consider the displacement constraint only. Then, Eq. (12) becomes

$$[L_1 + u_{1x}(L_1,t)]\boldsymbol{b}_{11} + u_{1y}(L_1,t)\boldsymbol{b}_{12} + u_{1z}(L_1,t)\boldsymbol{b}_{13} = \boldsymbol{R}_2 + [-L_2/2 + u_{2x}(-L_2/2,t)]\boldsymbol{b}_{21} + u_{2y}(-L_2/2,t)\boldsymbol{b}_{22} + u_{2z}(-L_2/2,t)\boldsymbol{b}_{23} \tag{50}$$

The augmented Lagrangian is

$$L' = K_1 + K_2 - V_1 - V_2 + \boldsymbol{\lambda} \cdot [-\boldsymbol{r}_1(E_1,t) + \boldsymbol{r}_2(B_2,t)] \tag{51}$$

where $\boldsymbol{\lambda} = (\lambda_1 \boldsymbol{b}_{21}\ \lambda_2 \boldsymbol{b}_{22}\ \lambda_3 \boldsymbol{b}_{23})^T$. Invoking the extended Hamilton's principle, we obtain a set of equations. The next step is to construct from this set the equations of motion by eliminating the Lagrange multipliers and R_{21}, R_{22}, and R_{23}. Note that, wherever they are referred to in further development, the range for the indices i, j, k, l, a, and b is as given below Eq. (39), and that for p, q, r, s, c, and d is as given following Eq. (47).

The resulting equations are very lengthy. Only the equations for θ_1 and one of the modal coordinates of link 1, $u_{1i}(i < N_{11})$ are presented here to examine the centrifugal stiffening and geometric softening effects. The equation for θ_1 is

$$\{I_1 + m_2 L_1^2 + m_{ij}^{(1)} u_{1i} u_{ij} - [\underline{h_{ab}^{(1)} + m_2 L_1 G_{ab}^{(1)}(L_1)}] u_{1a} u_{1b}\}\ddot{\theta}_1 + m_2 \left\{ \left[\frac{L_1 L_2}{2} + \frac{L_1}{2} G_{cd}^{(2)}\left(\frac{-L_2}{2}\right) u_{2c} u_{2d} - 0.25\, L_2 \underline{G_{ab}^{(1)}(L_1) u_{1a} u_{1b}} - \phi_{1i}(L_1) u_{1i} \phi_{2p}\left(\frac{-L_2}{2}\right) u_{2p} \right] \cos(\theta_2 - \theta_1) + \left[L_1 \phi_{2p}\left(\frac{-L_2}{2}\right) u_{2p} + \frac{L_2}{2} \phi_{1i}(L_1) u_{1i} \right] \sin(\theta_2 - \theta_1) \right\} \ddot{\theta}_2 + \left\{ f_{1k} u_{1k} \cos\theta_1 - m_{ik}^{(1)} u_{1i} u_{1k} \sin\theta_1 + m_2 \left[L_1 \cos\theta_1 - \phi_{1i}(L_1) u_{1i} \sin\theta_1 \right] \left[-\phi_{2r}\left(\frac{L_2}{2}\right) u_{2r} + \phi_{1k}(L_1) u_{1k} \right] \right\} \ddot{\psi} + \left[f_{1i} + m_2 L_1 \phi_{1i}(L_1) \right] u_{1i} - m_2 L_1 \cos(\theta_2 - \theta_1) \phi_{2p}\left(\frac{L_2}{2}\right) u_{2p} + A = F_{\theta 1} \tag{52}$$

where $F_{\theta 1}$ is the rigid-body torque.

The equation for $u_{1i}(i \le N_{11})$ is

$$\left[m_{ij}^{(1)} + m_2 \phi_{1i}(L_1) \phi_{1j}(L_1) \right] \ddot{u}_{1j} - \left[m_2 \phi_{1i}(L_1) \phi_{2p}\left(\frac{-L_2}{2}\right) \cos(\theta_2 - \theta_1) \right] \ddot{u}_{2p} + [f_{1i} + m_2 L_1 \phi_{1i}(L_1)] \ddot{\theta}_1 + m_2 \left\{ \left[\left(\frac{L_2}{2}\right) \underline{G_{ib}^{(1)}(L_1) u_{1b}} + \phi_{1i}(L_1) \phi_{2p}\left(-\frac{L_2}{2}\right) u_{2p} \right] \sin(\theta_2 - \theta_1) + \left(\frac{L_2}{2}\right) \phi_{1i}(L_1) \cos(\theta_2 - \theta_1) \right\} \ddot{\theta}_2 + \left\{ m_{ik}^{(1)} u_{1k} + m_2 \phi_{1i}(L_1) \left[-\phi_{2r}\left(\frac{-L_2}{2}\right) u_{2r} + \phi_{1k}(L_1) u_{1k} \right] \right\} \cos\theta_1 \ddot{\psi} + \left\{ k_{ij}^{(1)} + \underline{h_{ij}^{(1)}} (\dot{\theta}_1^2 + \dot{\psi}^2 \sin^2\theta_1) - m_{ij}^{(1)} (\dot{\theta}_1^2 + \dot{\psi}^2 \cos^2\theta_1) + \underline{m_2 G_{ij}^{(1)}(L_1)} \left[L_1 \dot{\theta}_1^2 + \left(\frac{L_2}{2}\right) \dot{\theta}_2^2 \cos(\theta_2 - \theta_1) + g \cos\theta_1 \right] - m_2 \phi_{1i}(L_1) \phi_{1j}(L_1) \dot{\theta}_1^2 + \underline{m_2 G_{ij}^{(1)}(L_1)} (L_1 \sin\theta_1 + \left(\frac{L_2}{2}\right) \sin\theta_2) \sin\theta_1 \dot{\psi}^2 - m_2 \phi_{1i}(L_1) \phi_{1j}(L_1) \cos^2\theta_1 \dot{\psi}^2 \right\} u_{1j} + D_i = F_{1i}, \quad i = 1,2,\ldots N_{11} \tag{53}$$

from Eq. (11)

$$F_{1i} = \int M(x,t) \phi_i'(x) \delta(x)\, dx = F_{\theta 1} \phi_i'(0)$$

A and D_i contain the Coriolis, centrifugal, and gravity terms. Note that the centrifugal stiffening effect as represented by $h_{ij}^{(1)}$ and $G_{ij}^{(1)}$ not only serves to increase the stiffness of the link [shown underlined in Eqs. (52) and (53)], but affects the rigid-body motion of the link as well.

The question then arises about the geometric effects, as represented by the terms with negative sign in the coefficient of u_{1j} in Eq. (53), and which one of them—"stiffening" or "softening"—has a more significant effect on the total motion. To investigate this, we consider a single link pinned at one end and free to rotate in a horizontal plane. The equations of motion are obtained by setting all of the elements corresponding to the second link, and all of the modal coordinates corresponding to vibration in a plane perpendicular to the plane of rotation of the link, equal to zero in Eqs. (52) and (53).

The dimensions of the link are taken as similar to those of a beam used at NASA Langley for structural control experiments.[28] The link has a cross section of 15.24×0.952 cm ($6 \times 3/8$ in.) and is flexible only in the plane of rotation. The mass and stiffness properties are $m = 4.015$ kg/m, $EI = 756.65$ N/m^2, and it has a length $L = 3.657$ m (12 ft). The orthonormal eigenfunctions of a pinned-free beam are considered in the modal expansion. This choice was experimentally verified.[29] For the linear elastic model, $m_{ij} = \delta_{ij}$ and $k_{ij} = \omega_j^2 \delta_{ij}$, where δ_{ij} is the Kronecker delta and ω the natural frequencies by virtue of orthonormality of the trial functions. These diagonal elements along with the centrifugal stiffening coefficients h_{ij} are given in Table 1. The equations of motion for the rigid-body modes become

$$[I_1 + (m_{ij} - h_{ij}) u_{1i} u_{1j}] \ddot{\theta} + 2(m_{ij} - h_{ij}) u_{1i} \dot{u}_{1j} \dot{\theta} = F_{\theta 1} \tag{54}$$

Table 1 Comparison of h_{ij}, m_{ii}, and k_{ii}

	h_{ij}					
	$j = 1$	2	3	4	m_{ii}	k_{ii}
$i = 1$	6.397	1.861	−0.366	0.121	1.000	250.37
2	1.861	17.905	6.195	−1.480	1.000	2629.13
3	−0.366	6.195	35.999	12.635	1.000	11444.72
4	0.121	−1.480	12.635	60.673	1.000	33467.04

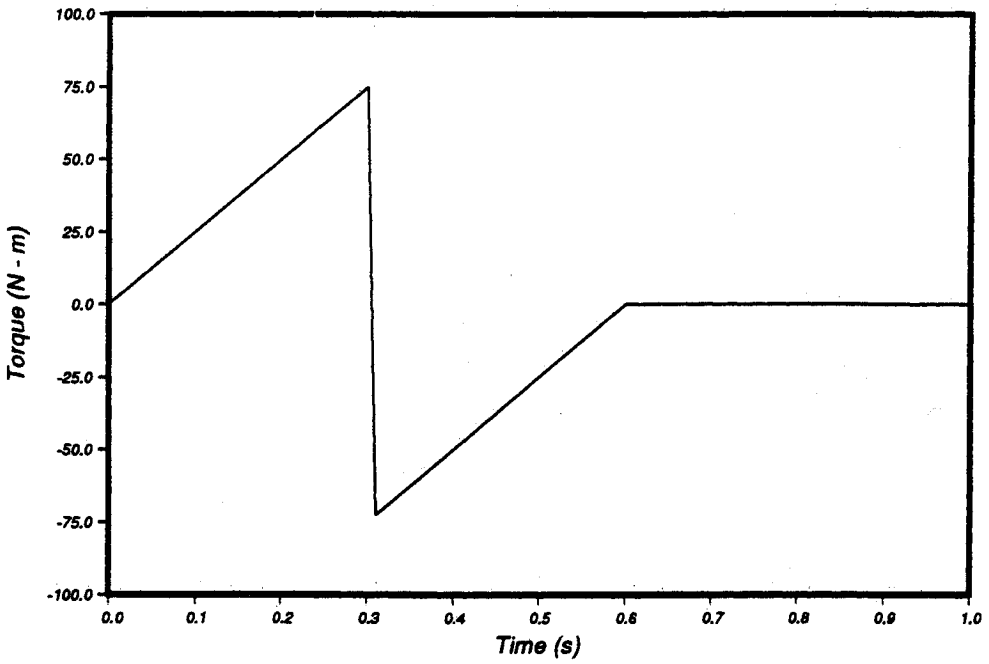

Fig. 5 Torque profile for open-loop maneuver.

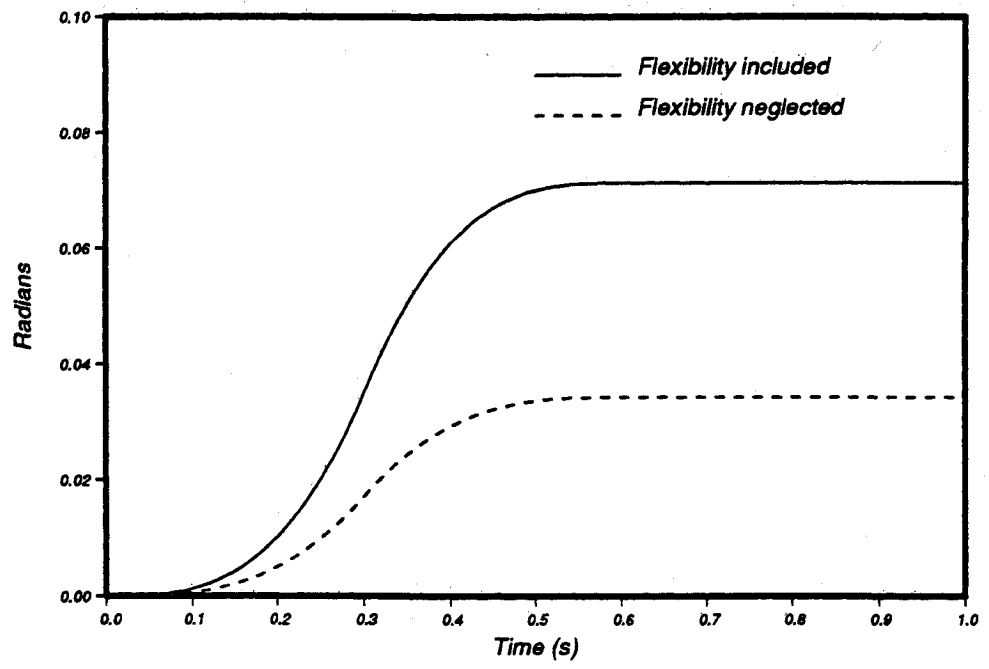

Fig. 6 Position response of the beam for the torque in Fig. 5.

and for the elastic modes

$$m_{ij}\ddot{u}_{1j} + [k_{ij} + (h_{ij} - m_{ij})\dot{\theta}^2]u_{1j} = F_{1i}, \qquad i = 1,2,\ldots N_{11} \quad (55)$$

The coefficient of $\ddot{\theta}$ ($M_{\theta\theta}$) in Eq. (54) is the time-varying inertia term, and the second term on the left side of the same equation represents the Coriolis effects. The centrifugal stiffening effect is apparent in the stiffness coefficients in Eq. (55) as well. Note that Eq. (54) can be written as

$$\frac{d}{dt}\{[I_1 + (m_{ij} - h_{ij})u_{1i}u_{1j}]\dot{\theta}\} = F_{\theta 1} \quad (56)$$

where the term

$$[I_1 + (m_{ij} - h_{ij})u_{1i}u_{1j}]\dot{\theta}$$

is recognized as the angular momentum of the link about the pin joint.

From Table 1 we observe that the diagonal terms corresponding to stiffening are much larger than the mass (or softening) terms. Hence, the difference $(h_{ij} - m_{ij})$ will be dominated by the former, and the centrifugal stiffening effect will be more pronounced than the softening effect for all values of $\dot{\theta}(t)$ and $\theta(t)$. This effect is present both in the rigid-body motion, Eq. (54), and in the elastic motion, Eq. (55). It is clear that rotation serves to stiffen an elastic structure. On the other hand, the same effect reduces the magnitude of the inertia terms in the rigid-body motion, thus increasing the angular velocity (for the same applied torque).

To demonstrate the effects of the centrifugal stiffening, we consider the following open-loop maneuver for the link: $\theta(0) = 0$, $\theta(T) = \theta_f$, $\dot{\theta}(T) = 0$, and T is the time of maneuver.

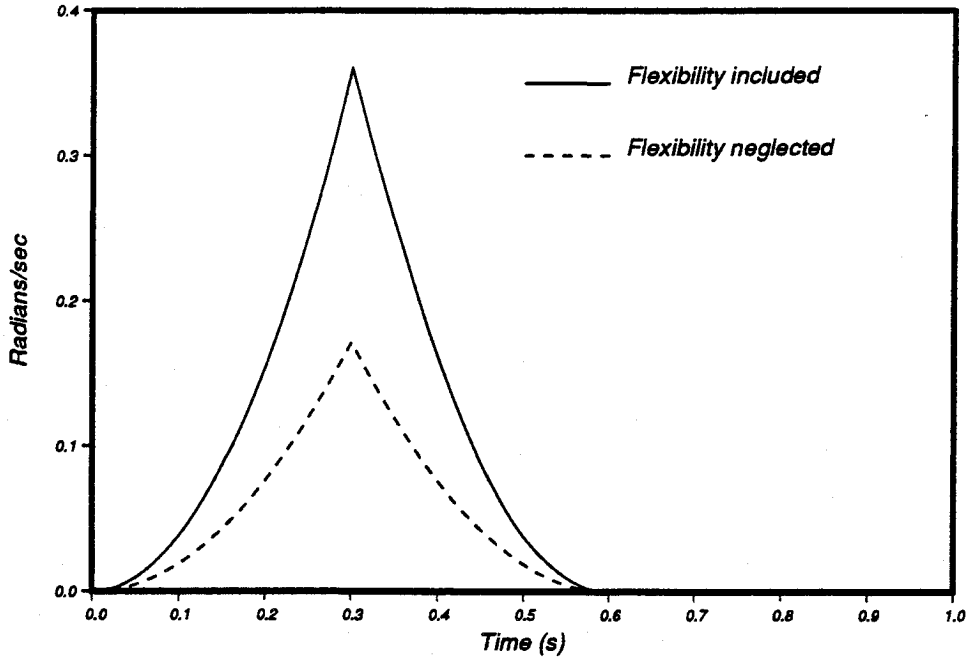

Fig. 7 Velocity response of the beam for the torque in Fig. 5.

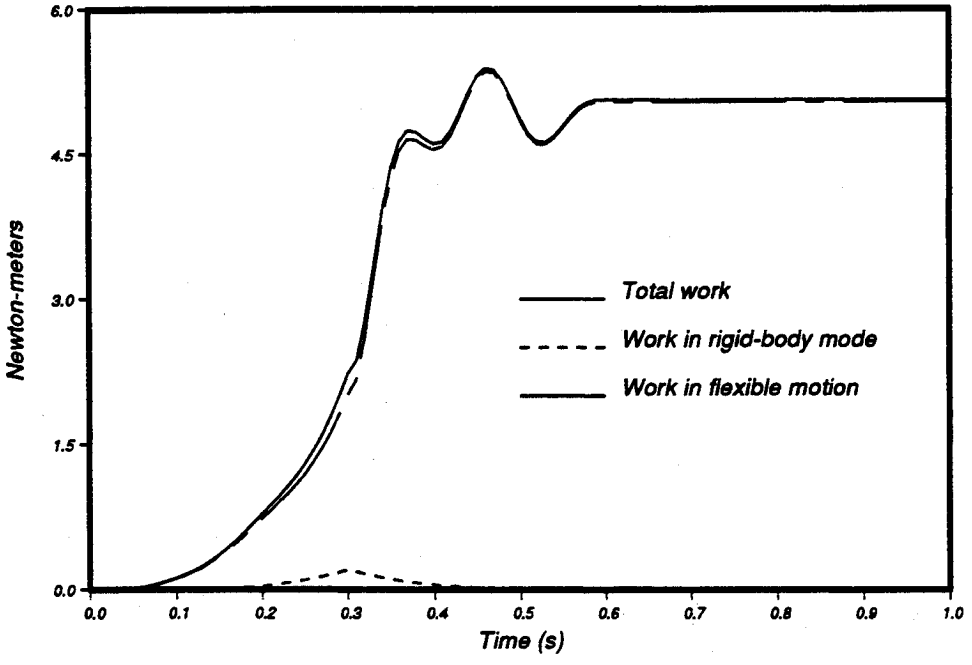

Fig. 8 Contribution of rigid and flexible modes to total work done.

We propose to achieve this with a torque profile shown in Fig. 5. From the double integral of $F_{\theta 1}/I$ and θ_f we obtain $F_{\theta 1}$. Three flexible modes are considered in the modal expansion, i.e., $N_{11} = 3$. Equations (54) and (55) are integrated using a fourth-order Runge-Kutta scheme with a time step of $0.001s$. The angular displacement $\theta(t)$ and velocity $\dot{\theta}(t)$ are plotted in Figs. 6 and 7, respectively, with their counterparts if flexibility was ignored. It is clear that the angular velocity is higher and $\theta(T) > \theta_f$ when flexibility is modeled. It was observed through system simulation that selecting the maneuver period T close to the period of the first natural frequency (of the small motions model) leads to violent vibrations, which was expected. Also, selection of a torque profile whose Fourier series expansion exhibits a Gibbs phenomenon, i.e., when the torque profile contains discontinuities, excited the elastic motion more.

Because of elasticity in the link, more work is needed to achieve θ_f than when flexibility is ignored. This is shown in Fig. 8 where the total energy in the link, which is equal to the amount of work done, energy in elastic motion, and energy in rigid-body motion, are plotted.

The work done, defined by $W(t)$, can be calculated by

$$W(t) = \int_0^t F_{\theta 1}(\sigma)\ [\dot{\theta}(\sigma) + \dot{u}'(0,\sigma)]\ d\sigma, \qquad 0 \le t \le T \quad (57)$$

The elastic motion of the tip of the link was observed to be the same both for the linear model and when centrifugal stiffening terms are modeled. The maximum tip deformation was observed to be 0.7 m, which is consistent with a small motions assumption for the elastic motion. We conclude that because of the large discrepancy in the rotation angles for the

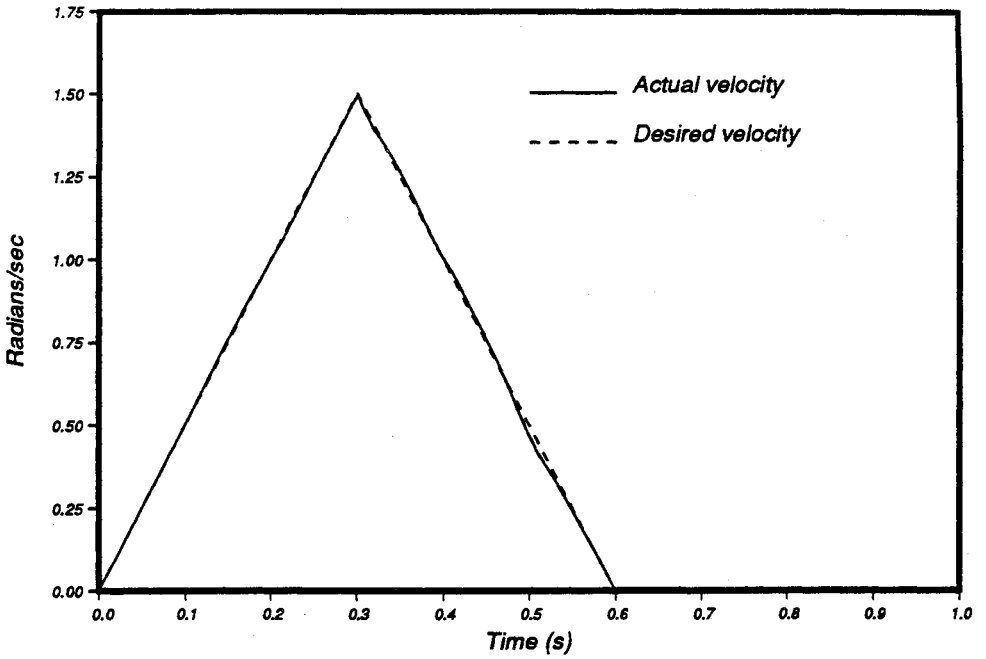

Fig. 9 Feedback control: rigid model, velocity response.

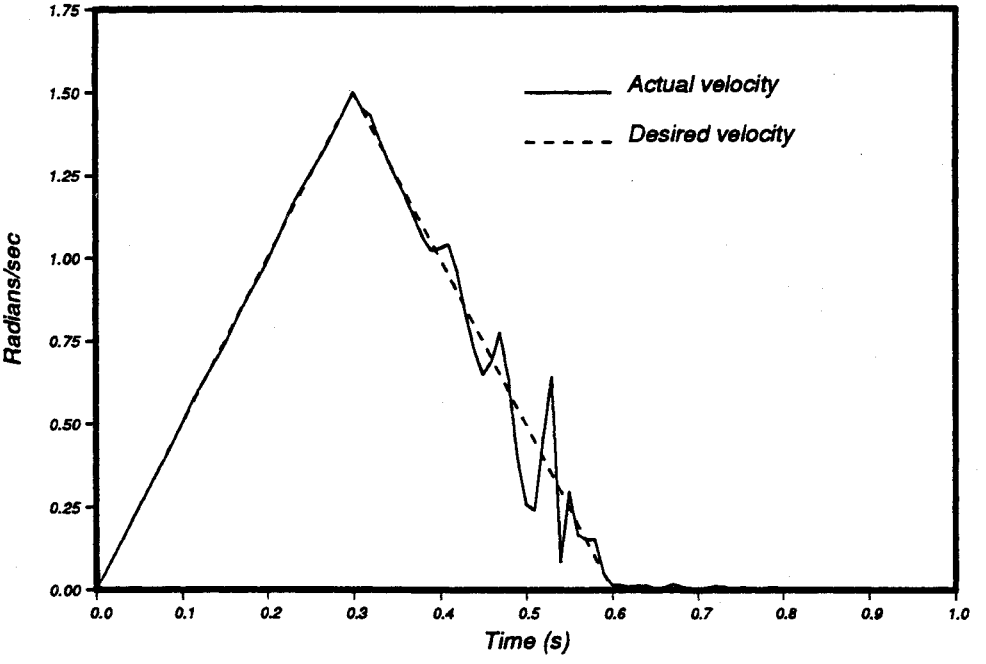

Fig. 10 Feedback control: one flexible mode included in the model.

different models, ignoring the centrifugal stiffening effects leads to gross inaccuracies.

Next, we consider the closed-loop control of the robot arm. We use a triangular shape for the desired angular velocity, i.e., $\dot{\theta}(t) = 5t$ rad/s, $0 < t \leq T/2$, $\dot{\theta}(t) = 5(0.6 - t)$ rad/s, $T/2 < t \leq T$, $T = 0.6$ s. The control law is based on the pointwise-optimal approach of Ref. 18, as given in Eq. (26). The elastic motion is not actively controlled, such that the model used for control is Eq. (29) where flexibility effects are included in the control design in various levels for comparison purposes. Note that for this particular example $M_{\theta v}$ is zero in Eq. (29). It is assumed that the effects of having a one time-step delay in the control application are eliminated by estimating the system state one time step earlier, as described in Ref. 18.

In the first case, the flexibility effects are totally ignored. The rigid model is considered as the actual one [$I_1\ddot{\theta}(t) = T(t)$] for control purposes, and the quantities that are fed back are the angle and time derivative of the angle at the pin joint, i.e., $q_1(t)$ and $\dot{q}_1(t)$, as given in Eq. (27). This approach leads to instabilities in the response, so that it was dropped as a viable form of control.

Next, the effects of flexibility were included in the model used for the control design. Initially, two sensors that measure the elastic deflection $u'(0,t)$ and $\dot{u}'(0,t)$ (one strain and one strain rate) were placed at the pin joint, in addition to the sensors that measure the total angular deflection $q_1(t)$ and its time derivative. From Eq. (27) the joint angle was calculated and introduced into the feedback loop as the difference of the measurements

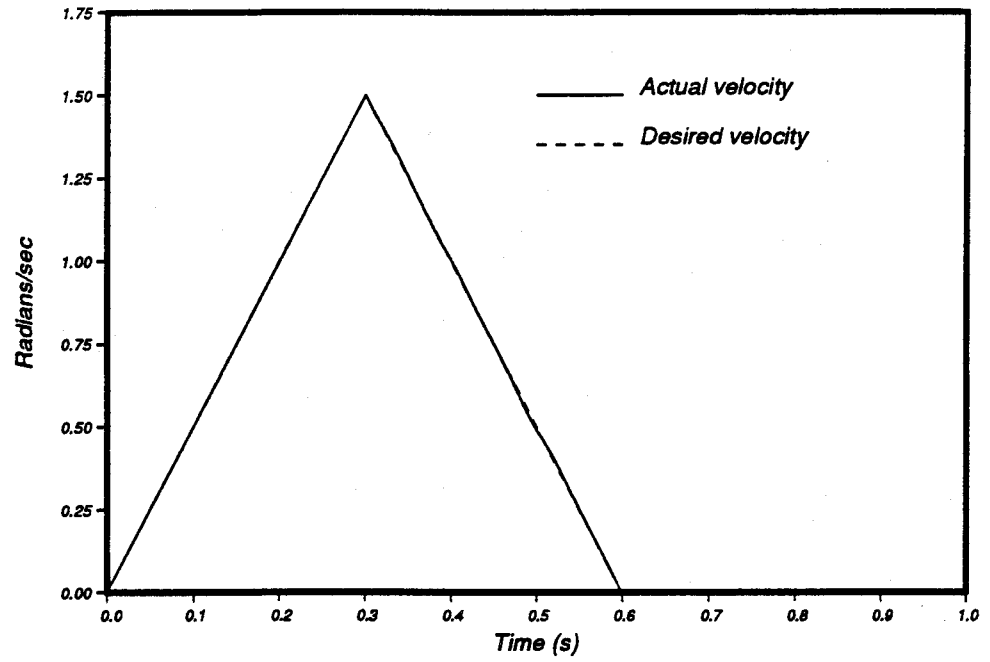

Fig. 11 Feedback control: three flexible modes included in the model.

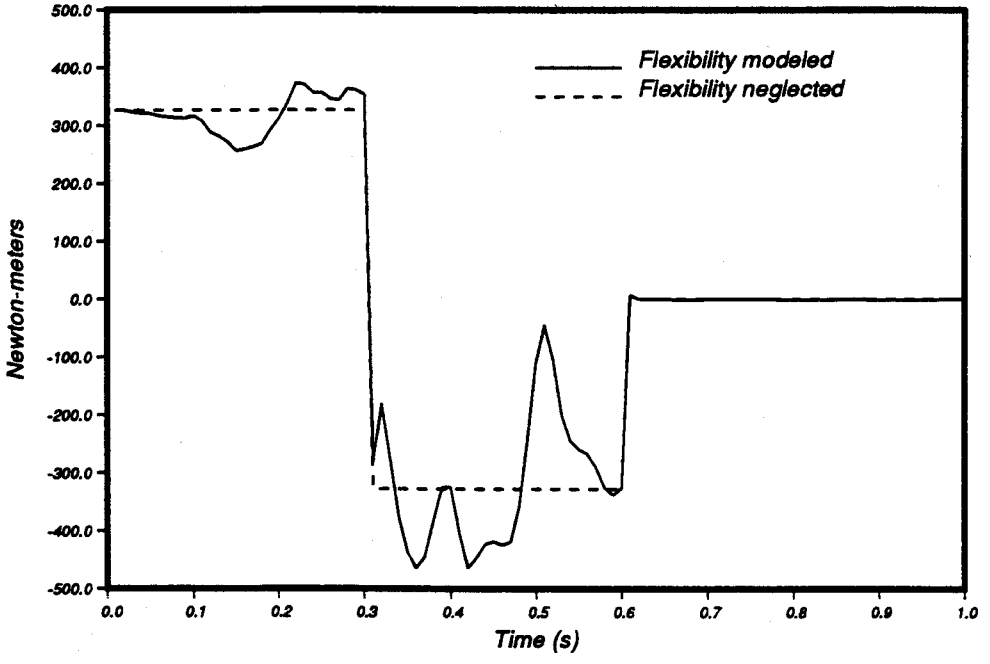

Fig. 12 Comparison of open- and closed-loop torques.

$$\theta(t) = q_1(t) - u'(0,t) \tag{58}$$

In the first approach, the rigid link was considered as the exact model, and the feedback quantities were calculated using Eq. (58). The response is plotted in Fig. 9. As can be seen, there is vast improvement over the open-loop case. In the second approach, the effects of elasticity are included in the mathematical model. By means of the expansion theorem, the elastic deflection can be expressed as

$$u'(x,t) = \phi_i'(x)u_{1i}(t) \tag{59}$$

Because only one sensor is available for displacements, we assume that the elastic displacement is due to the first mode only, and extract the first modal coordinate from the elastic motion measurements $u'(0,t)$ and $\dot{u}'(0,t)$ using

$$u_{11}(t) \approx u'(0,t)/\phi_1'(0), \qquad \dot{u}_{11}(t) \approx \dot{u}'(0,t)/\phi_1'(0) \tag{60}$$

The model on which the control inputs are based is Eq. (54), with the indices i,j taking the value of 1 only:

$$[I_1 + (m_{11} - h_{11})u_{11}^2]\ddot{\theta} + 2(m_{11} - h_{11})u_{11}\dot{u}_{11}\dot{\theta} = F_{\theta 1} \tag{61}$$

The response is shown in Fig. 10. We observe that the results of Fig. 9 are more accurate. This is because even though the control model used is more reliable than the rigid-body model, the errors associated with extraction of the modal

coordinates deteriorate the performance. These errors, of course, can be diminished by increasing the number of sensors and by improving the modal coordinate extraction process. Considering Eq. (59), the relation between the sensors output and modal coordinates can be expressed as

$$y(t) = [B_M B_R] \begin{Bmatrix} u_M(t) \\ u_R(t) \end{Bmatrix} \tag{62}$$

where the subscripts M and R denote the extracted (monitored) m and ignored (residual) $\infty - m$ modes; $y(t)$ is the output vector in the form $y(t) = [u'(x_1,t)u'(x_2,t)\ldots u'(x_m,t)]^T$ where x_j denote the sensors' locations. We extract as many modes as the number of sensors so that B_M becomes a square matrix, which can be shown to be nonsingular regardless of the sensors' locations.[16] The entries of B_M have the form $B_{Mij} = \phi_i(x_j)$. The entries of B_{Rij} are $B_{Rij} = \phi_{i+m}(x_j)$. The modal coordinates are extracted by ignoring the residual modes and by inverting B_M, which results in[30]

$$u(t) = u_M(t) + B_M^{-1} B_R u_R(t) \tag{63}$$

where $u(t)$ is the vector of extracted modal coordinates. The second term in the right side of Eq. (63) denotes the estimation error. A more sophisticated form of extraction of modal coordinates is by use of modal filters and modal observers,[16,30] which minimizes the errors associated with ignoring the residual modes.

To improve the accuracy of the modal coordinate extraction, we increase the number of sensors used to measure the elastic motion. Figure 11 shows the results of applying the closed-loop control law using three spatially distributed sensors for the strains and strain rates. As may be observed from Fig. 11, the results are greatly improved, which is to be expected. Figure 12 shows the torque profile and compares it with the torque that would have been required if the bar were assumed to be rigid. The deviations are caused by the elastic effects.

The above results were obtained for the case when the maximum value of the desired velocity was 1.5 rad/s. When the desired rotational speeds and maximum angular velocity were increased substantially, for a triangular velocity profile, the simulation results were not accurate. This is because the higher slope for the velocity profile (especially a nonzero slope at $t = 0$) requires larger magnitudes for the applied torque, which excites the elastic motion substantially and causes it to reach large magnitudes. This forces the first term in Eq. (54), which is the coefficient of $\ddot{\theta}(t)$ and, thus, a measure of the moment of inertia, to become very small. We conclude that when the applied torque is very large, the elastic motion grows rapidly, and under such circumstances the accuracy of the maneuver deteriorates. Also, the small motions assumption may begin to lose its validity. The elastic motion then has to be modeled using another approach, such as in Ref. 31. Actually, one can check the limits of the small motions assumption for elastic bodies undergoing rapid rigid-body motion by examining the magnitude of the first term in Eq. (54).

The small motions assumption will be valid if high angular velocities are approached by applying a torque gradually, which does not excite the elastic motion as much. To examine this, the preceding simulations were also carried out when the desired angular displacement and velocity were chosen the same as the open-loop maneuver described earlier. For this case, because the torque is applied gradually (compare Figs. 6 and 12), the elastic motion was not excited as much. Consequently, much higher angular velocities could be prescribed in which the small elastic motions assumption was not violated. Also, because the magnitude of the elastic motion was not large, using one sensor or three sensors to measure the elastic motion yielded almost the same accuracy, where the desired angular profile was followed extremely closely.

VI. Discussion

We have presented in this paper issues associated with modeling and control of robots with relative elasticity in their arms. An approach similar to the component mode and substructure synthesis methods is proposed to derive the equations of motion, and several control strategies are discussed. It is shown that the centrifugal stiffening effect is more significant than the geometric softing effect. The centrifugal stiffening affects both the elastic and the rigid-body motions, causing a loss in inertia and an increase in the angular velocities. Both the open-loop and closed-loop control of the manipulator arm are considered, where in the latter the feedback quantities are calculated by using the output of spatially distributed sensors.

References

[1]Book, W. J., "Analysis of Massless Elastic Chains with Servo Controlled Joints," *Journal of Dynamic Systems, Measurement, and Control,* Vol. 101, Sept. 1979, pp. 187–192.

[2]Judd, R. P. and Falkenburg, D. R., "Dynamics of Non-Rigid Articulated Robot Linkages," *IEEE Transactions on Automatic Control,* Vol. AC-30, May 1985, pp. 499–502.

[3]Zalucky, A. and Hardt, D. E., "Active Control of Robot Structure Deflections," *Journal of Dynamic Systems, Measurement, and Control,* Vol. 106, March 1984, pp. 63–69.

[4]Kelly, F. A. and Huston, R. L., "Modeling Flexibility Effects in Robot Arms," *Proceedings of the 1981 Joint Automatic Control Conference,* Paper WP-2C, June 1981.

[5]Sunada, W. H. and Dubowsky, S., "On the Dynamic Analysis and Behavior of Industrial Robotic Manipulators with Elastic Members," *Journal of Mechanisms, Transmissions, and Automation in Design,* Vol. 105, March 1983, pp. 42–51.

[6]Midha, A., Erdman, A. G., and Frohrib, D. A., "Finite-Element Approach to Mathematical Modeling of High-Speed Elastic Linkages," *Mechanisms and Machine Theory,* Vol. 13, 1978, pp. 603–618.

[7]Chang, L.-W., "Dynamic Analysis of Robotic Manipulators with Flexible Links," Ph. D. Thesis, Purdue Univ., West Lafayette, IN, 1984.

[8]Alberts, T. E., Hastings, G. G., Book, W. J., and Dickerson, S. L., "Experiments in Optimal Control of a Flexible Arm with Passive Damping," *Proceedings of the Fifth VPI&SU/AIAA Symposium on Dynamics and Control of Large Structures,* AIAA, New York, 1985, pp. 423–436.

[9]Chalhoub, N. G. and Ulsoy, A. G., "Dynamic Simulation of a Flexible Arm and Controller," *ASME Journal of Dynamic Systems, Measurement, and Control,* Vol. 108, June 1986, pp. 119–126.

[10]Book, W. J., "Recursive Lagrangian Dynamics of Flexible Manipulator Arms Via Transformation Matrices," *International Journal of Robotics Research,* Vol. 3, Fall 1984, pp. 87–101.

[11]Dubowsky, S. and Gardner, T. N., "Design and Analysis of Multilink Flexible Mechanisms with Multiple Clearance Connections," *Journal of Engineering for Industry,* Vol. 99, No. 1, Feb. 1977, pp. 88–96.

[12]Spong, M. W., "Modeling and Control of Elastic Joint Robots," *Proceedings of ASME 1986 WAM: Robotics, Theory and Applications,* American Society of Mechanical Engineers, New York, 1986.

[13]Silverberg, L. M. and Baruh, H., "Simultaneous Maneuver and Vibration Suppression of Flexible Spacecraft," *Applied Mathematical Modelling,* Vol. 12, Dec. 1988, pp. 546–555.

[14]Baruh, H. and Silverberg, L. M., "Implementation Problems Associated with Simultaneous Maneuver and Vibration Suppression of Flexible Spacecraft," *Proceedings of the Fifth VPI&SU/AIAA Symposium on Dynamics and Control of Large Structures,* AIAA, New York, 1985, pp. 585–599.

[15]Meirovitch, L., *Computational Methods in Structural Dynamics,* Sijthoff-Noordhof, The Netherlands, 1980.

[16]Meirovitch, L. and Baruh, H., "Control of Self-Adjoint Distributed-Parameter Systems," *Journal of Guidance, Control, and Dynamics,* Vol. 5, Jan.–Feb. 1982, pp. 60–66.

[17]Spong, M. W., Thorp, J. S., and Kleinwaks, J. M., "The Control of Robot Manipulators with Bounded Input," *IEEE Transactions on Automatic Control,* Vol. 31, No. 6, 1986, pp. 483–490.

[18]Tadikonda, S. and Baruh, H., "Pointwise-Optimal Control of Robot Manipulators," *ASME Journal of Dynamic Systems, Measurement, and Control,* Vol. 110, No. 2, June 1988, pp. 210–213.

[19]Singh, S. N. and Schy, A. A., "Control of Elastic Robotic Systems by Nonlinear Inversion and Modal Dampings," *Journal of Dynamic Systems, Measurement, and Control,* Vol. 108, Sept. 1986, pp. 180–189.

[20]Laskin, R. A., Likins, P. W., and Longman, R. W., "Dynamical Equations of a Free-Free Beam Subject to Large Overall Motions," *Journal of Astronautical Sciences,* Vol. 31, No. 4, Oct.-Dec. 1983, pp. 507-527.

[21]Canavin, J. R. and Likins, P. W., "Floating Reference Frames for Flexible Spacecraft," *Journal of Spacecraft,* Vol. 14, Dec. 1977, pp. 724-732.

[22]Smith, C. D., "Response Simulation and Control of an Unconstrained Structure Subject to Large Overall Motions," M.S. Thesis, Rutgers Univ. New Brunswick, NJ, May 1988.

[23]Meirovitch, L., *Methods of Analytical Dynamics,* McGraw-Hill, New York, 1969.

[24]Craig, R. R., Jr. and Bampton, M. C. C., "Coupling of Substructures for Dynamic Analysis," *AIAA Journal,* Vol. 6, July 1968, pp. 1313-1319.

[25]Hale, A. L. and Meirovitch, L., "A General Substructure Synthesis Method for the Dynamic Simulation of Complex Structures," *Journal of Sound and Vibration,* Vol. 69, No. 2, March 1980, pp. 309-326.

[26]Luh, J. Y. S., Walker, M. W., and Paul, R. P. C., "Resolved Acceleration Control of Mechanical Manipulators," *IEEE Transactions on Automatic Control,* Vol. AC-25, June 1980, pp. 469-474.

[27]Kane, T. R. and Ryan, R. R., "Dynamics of a Cantilever Beam Attached to a Moving Base," *Journal of Guidance, Control, and Dynamics,* Vol. 10, March-April, 1987, pp. 139-151.

[28]Meirovitch, L., Baruh, H., Montgomery, R. C., and Williams, J. P., "Nonlinear Natural Control of an Experimental Beam," *Journal of Guidance, Control, and Dynamics,* Vol. 7, July-Aug., 1984, pp. 437-442.

[29]Cannon, R. H., Jr. and Schmitz, E., "Initial Experiments on the End-Point Control of a Flexible One-Link Robot," *The International Journal of Robotics Research,* Vol. 3, No. 3, Fall 1984, pp. 62-75.

[30]Meirovitch, L. and Baruh, H., "Implementation of Modal Filters for Control of Structures," *Journal of Guidance, Control, and Dynamics,* Vol. 8, Nov.-Dec., 1985, pp. 707-716.

[31]Simo, J. C. and Vu-Quoc, L., "The Role of Nonlinear Theories in Transient Dynamic Analysis of Flexible Structures," *Journal of Sound and Vibration,* Vol. 119, No. 3, Dec. 1987, pp. 487-508.